MAPPING TIDAL CURRENTS AND RESIDUAL CURRENTS BY USE OF COASTAL ACOUSTIC TOMOGRAPHY

Xiao-Hua Zhu, State Key Laboratory of Satellite Ocean Environment Dynamics, Second Institute of Oceanography, State Oceanic Administration, China
Ze-Nan Zhu, State Key Laboratory of Satellite Ocean Environment Dynamics, Second Institute of Oceanography, State Oceanic Administration, China
Xinyu Guo Center for Marine Environmental Study, Ehime University, 2-5 Bunkyo-cho, Matsuyama 790-8577, Japan

xhzhu@sio.org.cn

A coastal acoustic tomography (CAT) experiment for mapping the tidal currents in the Zhitouyang Bay was successfully carried out with seven acoustic stations during July 12 to 13, 2009. The horizontal distributions of tidal current in the tomography domain are calculated by the inverse analysis in which the travel time differences for sound traveling reciprocally are used as data. Spatial mean amplitude ratios M_2 : M_4 : M_6 are 1.00 : 0.15 : 0.11. The shallow-water equations are used to analyze the generation mechanisms of M_4 and M_6. In the deep area, velocity amplitudes of M_4 measured by CAT agree well with those of M_4 predicted by the advection terms in the shallow water equations, indicating that M_4 in the deep area where water depths are larger than 60 m is predominantly generated by the advection terms. M_6 measured by CAT and M_6 predicted by the nonlinear quadratic bottom friction terms agree well in the area where water depths are less than 20 m, indicating that friction mechanisms are predominant for generating M_6 in the shallow area. Dynamic analysis of the residual currents using the tidally averaged momentum equation shows that spatial mean values of the horizontal pressure gradient due to residual sea level and of the advection of residual currents together contribute about 75% of the spatial mean values of the advection by the tidal currents, indicating that residual currents in this bay are induced mainly by the nonlinear effects of tidal currents.

Key words: tidal current structures, residual currents, M_4 and M_6 generation mechanisms, coastal acoustic tomography

I. INTRODUCTION

The continuous monitoring of tidal currents in bays, inland seas, and straits over a large area is difficult, especially in the coastal seas of China, where fishing and shipping pressures are high. Furthermore, in order to examine generation mechanisms of the nonlinear tidal currents, the 2-dimensional continuous current field also should be mapped accurately to allow calculation of the advection terms.

To obtain observations of rapidly varying tidal current structures, bottom-mounted or subsurface moored current meter arrays are needed as conventional tools. However, heavy shipping traffic and fishery activities make it difficult to deploy such mooring arrays in almost all coastal regions in China, even if the antitrawl bottom-mounted acoustic Doppler current profiler (ADCP) systems are applicable. Coastal Acoustic Tomography (CAT) can achieve this easily by deploying only a few instruments on the periphery of the observation region [1]-[2].

II. SITE AND METHOD

An experiment with seven CAT systems was performed on July 12–13, 2009, in a neap tidal period at Zhitouyang Bay (hereinafter ZTYB) near Zhoushan Island around the mouth of Hangzhou Bay, China (Fig. 1).

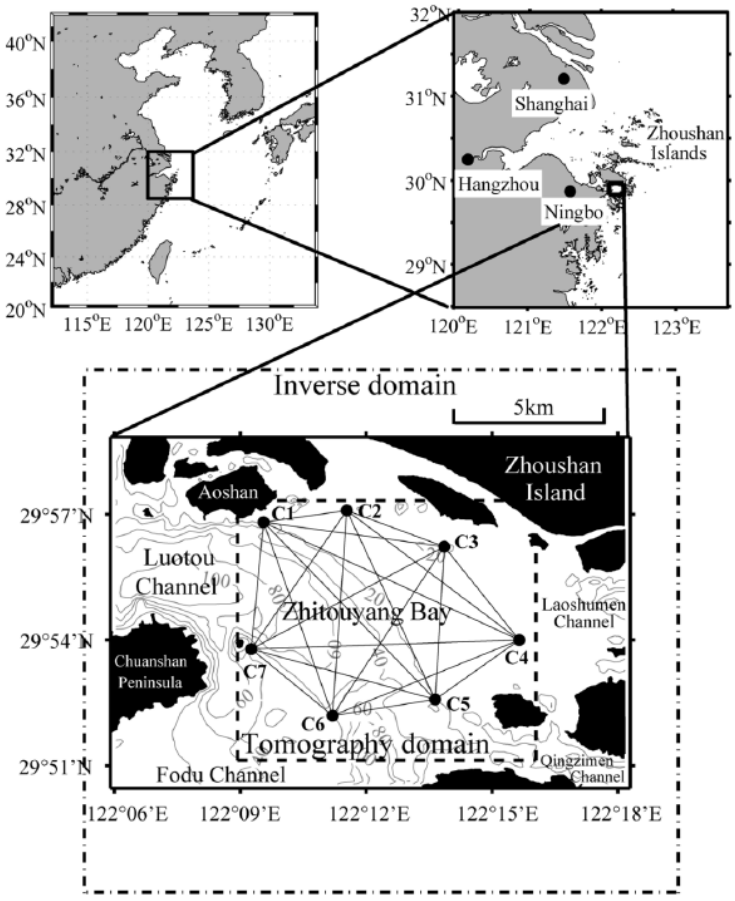

Fig. 1 Location maps of the experimental site. The positions of the CAT stations (C1–C7) are shown with solid circles. The thick solid lines connecting the CAT stations indicate the sound transmission lines. The interval of bathymetric contours is 20 m.

The seven CAT systems were set up at seven stations numbered C1–C7 using fishing boats anchored on the periphery of the bay. The transducer was suspended down to 5–10 m depths from the boat by rope, while the major components of the system, such as electronic housing, batteries, and Global Positioning System (GPS) antennas were put onboard the boat.

For the geographical configuration of acoustic stations, the total number of transmission lines of 21 results in an average horizontal resolution of 1.8 km [3]. Grid size for the data display in the inverse analysis is set to be 1.0×1.0 km, which is slightly smaller than the horizontal resolution.

The inverse method developed by Park and Kaneko [3] is applied here to reconstruct the tidal current distributions by averaging any vertical dependency. The travel-time differences obtained from the reciprocal sound transmission for the CAT station pairs are used as data in the inverse analysis. The inverse domain is taken to be 22×22 km , which is twice the tomography

domain, to suppress the artificial periodicity of inverse results (Fig. 1). The equation for the inverse method is as follows:

$$\boldsymbol{y} = \boldsymbol{E}\boldsymbol{x} + \boldsymbol{e} \quad (1)$$

where $\boldsymbol{y}$ is a 21-element column vector, each column denotes the travel-time difference data of each station pair; $\boldsymbol{x}$ is a vector of the 20-element row vector of the unknown coefficients used in the Fourier function expansion of the stream function used to estimate the current field; $\boldsymbol{E}$ is a 21×20 matrix, determined by the locations of the 7 CAT stations; $\boldsymbol{e}$ is the error vector. The optimum solution of (1) is obtained by minimizing the objective function ($\boldsymbol{J}$) with the tapered least squares method. The objective function is given by:

$$\boldsymbol{J} = (\boldsymbol{y} - \boldsymbol{E}\boldsymbol{x})^T(\boldsymbol{y} - \boldsymbol{E}\boldsymbol{x}) + \alpha^2\boldsymbol{x}^T\boldsymbol{x} \quad (2),$$

where the weighting factor α is determined by the L-curve method [4].

After obtaining the current field at each spatial grid point for a period of 27 hours by using the inverse method, we then compute the M_2, M_4 and M_6 harmonic constants at each grid point by using harmonic tidal analysis [5].

To obtain the M_4 and M_6 tidal currents generated by the advection terms ($u\frac{\partial u}{\partial x} + v\frac{\partial u}{\partial y}$ and $u\frac{\partial v}{\partial x} + v\frac{\partial v}{\partial y}$) and quadratic bottom friction terms ($\frac{C_d}{h+\eta}u\sqrt{u^2+v^2}$ and $\frac{C_d}{h+\eta}v\sqrt{u^2+v^2}$), we firstly substitute the tidal current forms of M_2 into the advection terms and quadratic bottom friction terms of the shallow water equations, respectively. Then, we obtain the terms having the M_4 and M_6 frequencies as the predicted M_4 and M_6 tidal currents (hereinafter M_{4_cal} and M_{6_cal}). Comparing the predicted M_4 and M_6 currents with those observed directly by CAT, we can quantify the contribution of advection terms and quadratic bottom friction terms for generating M_4 and M_6 [6].

III. RESULTS AND DISCUSSION

A. Horizontal distribution of tidal current

The inversion results provide synoptic snapshots of horizontal tidal current distributions at hourly intervals. The hourly mean tidal current structures from 18:00:00 July 12, 2009 to 17:00:00 July 13, 2009, are shown in Fig. 2. The strong eastward tidal current, with a maximum current of 2.05 m/s, entered the tomography site from the Luotou channel at the western part of the bay and separated into two branches flowing into the Laoshumen channel and the Qingzimen and Fodu channels during the ebb tide (Fig. 2a–2c). During the flood tide, the strong westward tidal current, with a maximum current of 1.03 m/s, merged with the currents from the Laoshumen, Qingzimen, and Fodu channels and went back to the Luotou channel during the flood tide (Fig. 2f–2h). This tidal current variation was repeated at the half-day cycle.

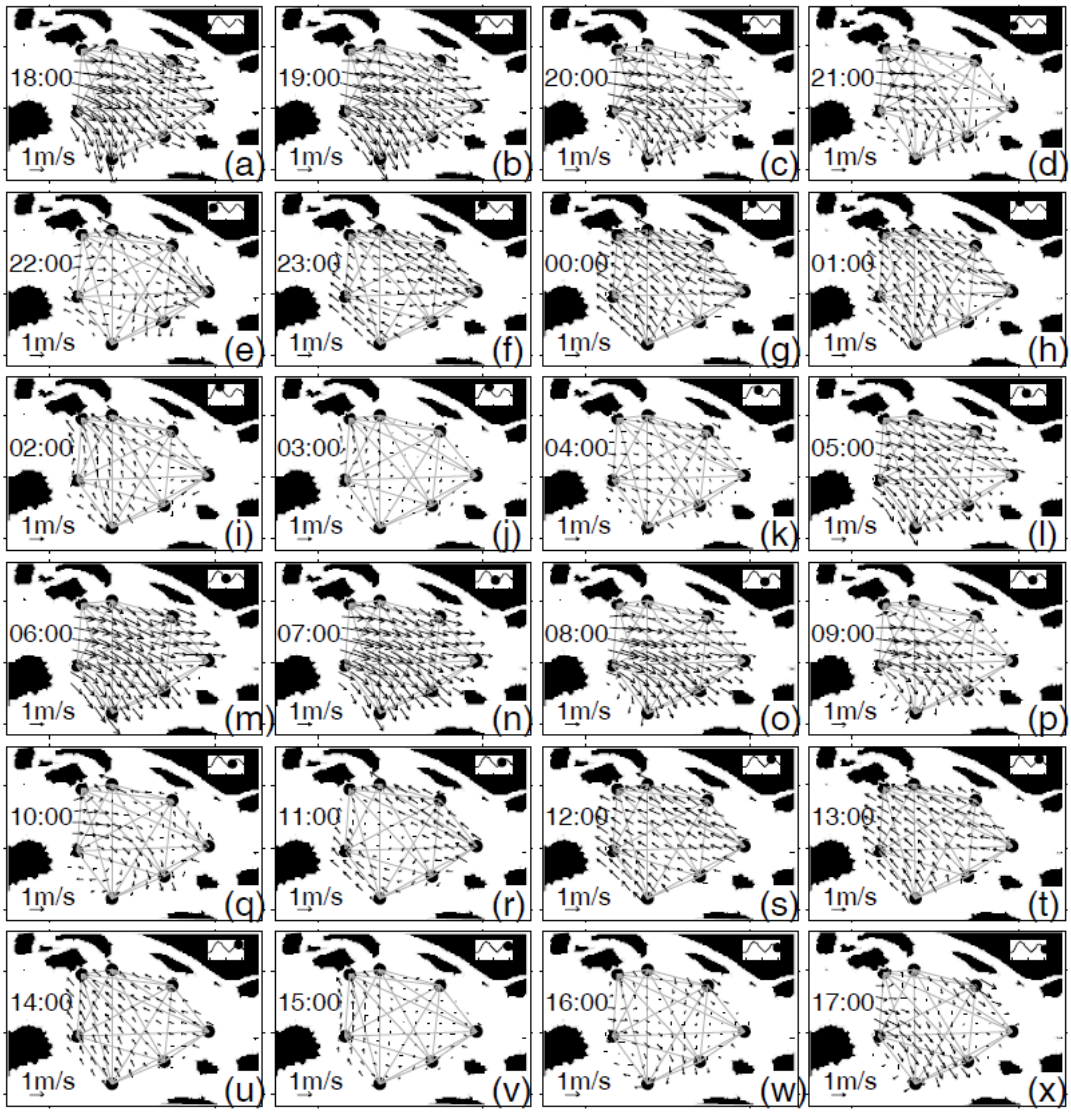

Fig. 2 Vector plots of the hourly mean current reconstructed from 18:00:00 July 12, 2009 to 17:00:00 July 13, 2009, by the inverse analysis. The tidal phases are indicated by a dot on the sea surface height (SSH) plot at the upper right of each panel.

B. Harmonic analysis of tidal currents

The harmonic analysis showed that the M_2 tide was the predominant tidal constituent. The semimajor axes of the tidal ellipse were directed to the east–west at the western half of the site and were separated into two directions at the eastern half (Fig. 3a). The mean semimajor and semiminor axes of the tidal ellipses were 1.00 and 0.07 m/s, respectively. The vector plot of the residual current is shown in Fig. 3b. The residual current was strong near the Luotou channel and became weak in the eastern part of the bay. The residual current flowed out as the eastward current from the Luotou channel and then turned southward along the 40-m bathymetric contour in the middle of the site.

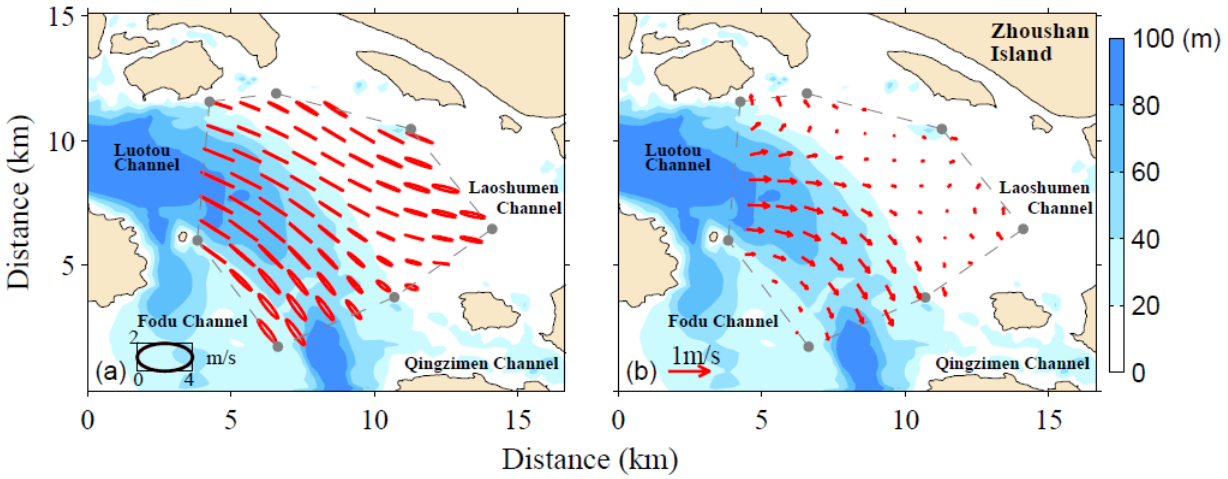

Fig. 3 The distribution of (a) M_2 tidal current ellipses, and (b) residual currents in Zhitouyang Bay. The gray solid circles are the positions of the CAT stations (C1-C7). The area enclosed by the dashed lines indicates the CAT observational region.

The spatially-averaged amplitude ratios M_2 : M_4 : M_6 are 1.00 : 0.15 : 0.11. The relatively large M_4 and M_6 overtides were observed in ZTYB. Then, we will discuss the generation mechanisms of M_4 and M_6 by using the ZTYB CAT data.

The horizontal distribution of the M_4 tidal ellipses measured by CAT and those of M_{4_cal} are shown in Fig. 4. The M_4 currents (Fig. 4a) are relatively large near the Luotou and Qinzimen channels with a maximum value 0.27 m s^{-1}, corresponding well to the distribution of the M_2 tidal current (Fig.3a). The area averaged semimajor and semiminor axis lengths of the M_4 tidal ellipses are 0.15 and 0.04 m/s, respectively (Table 1). The spatial mean ellipticity of the M_4 tide is 0.27, which is larger than that of M_2 (0.07). The M_{4_cal} currents (Fig. 4b) are also relatively large near the Luotou and Qinzimen channels with a maximum value 0.32 m/s near Luotou channel. The M_{4_cal} ellipses have the same area averaged semimajor and semiminor axis lengths as the observed M_4 values (Table 1).

The M_4 semimajor axis direction is mainly northeast-southwest in the west part of the observation region, and becomes northwest-southeast in the east part (Fig. 4a). The M_{4_cal} semimajor axis direction is mainly northeast-southwest in the west part of the region, and becomes north-south in the east part (Fig. 4b).

We compare the velocity amplitudes of M_4 and M_{4_cal} to confirm the contribution of advection terms in generating the M_4 tide in different areas of the observational region. We consider the M_4_and M_{4_cal} ellipses to be similar at those points (red ellipses in Fig. 4) for which the differences of both velocity amplitude and phase between M_4_and M_{4_cal} are less than one STD of the differences between the M_4_and M_{4_cal} values, i.e., 0.07m s^{-1} and 110º, respectively. We find that the tidal current ellipses are most similar in the deep area where water depths are larger than 60 m. The distribution of M_2 ellipses (Fig.3a) shows that relatively large M_2 currents appear in the deep area, which means the values of the advection terms are also larger in the deep area. Thus the advection terms make a primary contribution to M_4 generation in the deep area. Moreover the tidal current ellipses (black ellipses in Fig. 4) are not generally similar in shallow waters, that is to say the M_4 tidal currents in the shallow area are not mainly caused by the advection terms. There are other key factors for generating M_4 in the shallow area, such as the continuity terms or the friction mechanism [7].

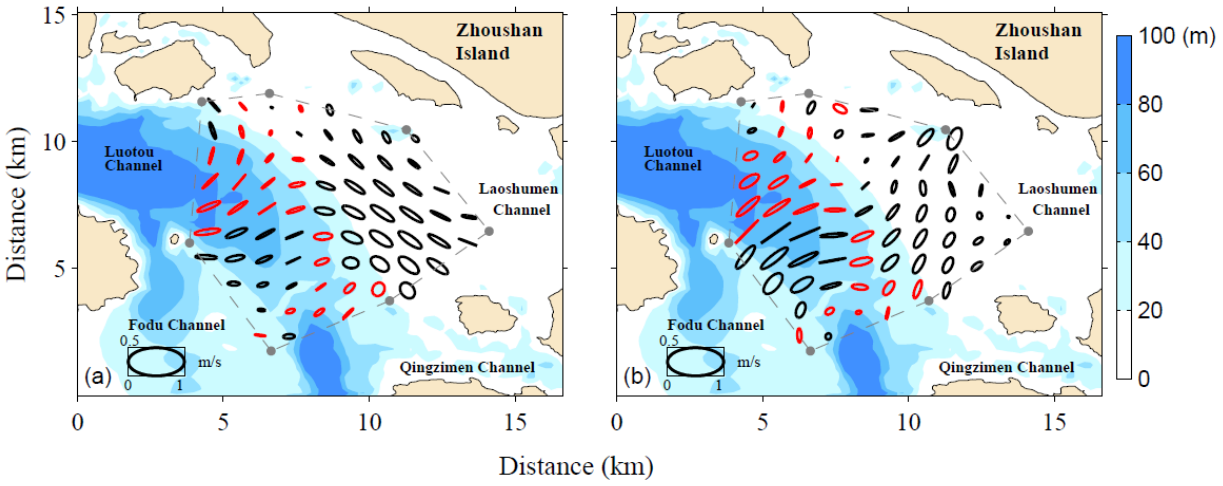

Fig. 4 Tidal current ellipses of (a) M_4, and (b) M_{4_cal}. Red lines indicate similar ellipses for M_4 and M_{4_cal}. The area enclosed by the dashed lines indicates the CAT observational region.

The horizontal distribution of the M_6 tidal ellipses measured by CAT and those of M_{6_cal} are shown in Fig. 5. The maximum value of the M_6 semimajor axes is 0.20 m/s, appearing near Luotou channel. The spatial mean semimajor and semiminor axis lengths of the M_6 current ellipses are 0.11 and 0.03 m/s (Table 1). The M_6 ellipticity is relatively small in the north part of the observational region, and becomes larger near Fodu channel. The spatial mean value of ellipticity is 0.27. The M_{6_cal} currents (Fig. 5b) are relatively larger near Luotou channel with a maximum value 0.10 m/s. The spatial mean semimajor and semiminor axis lengths of the M_{6_cal} tidal current ellipses are 0.07 and 0.01 m s^{-1}, respectively (Table 1). The spatial mean ellipticity of the M_{6_cal} tide is 0.09.

The orientations of the M_6 and M_{6_cal} tidal current ellipses correspond well throughout the observational region: both are mainly directed east-west in the north part of the observational region, and turn north-south along the 40 m bathymetric contour.

We further show the relationship of M_6_and M_{6_cal} velocity amplitudes to confirm the contribution of the quadratic bottom friction terms to the generation of M_6 in different areas of the observational region. We consider the M_6 and M_{6_cal} ellipses to be similar at those points (red ellipses in Fig. 5) for which the difference of velocity amplitude between M_6_and M_{6_cal} is less than the STD of the differences between the M_6_and M_{6_cal} values (i.e., 0.05m s^{-1}). Where the tidal current ellipses are similar (red ellipses in Fig. 5) this similarity indicates M_6 mainly generated by the quadratic bottom friction terms; this occurs principally in the east part of the observational region where water depth is less than 20 m. These results indicate that the quadratic bottom friction terms play a primary role for generating M_6 in shallow waters, while M_6 in the deep area is also affected by such factors such as the other nonlinear terms in the momentum equations [8].

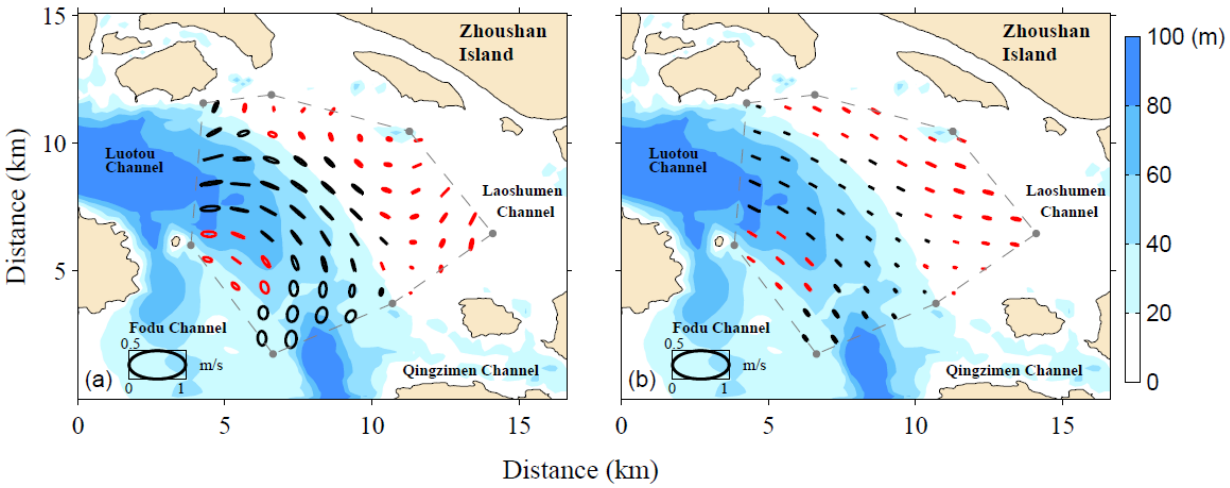

Fig. 5 Tidal current ellipses of (a) M_6, and (b) M_{6_cal}. Red lines indicate similar ellipses for M_6 and M_{6_cal}. The area enclosed by the dashed lines indicates the CAT observational region.

Table 1. Spatial mean parameters of tidal current ellipses of M_4, M_{4_cal}, M_6, M_{6_cal} and their STDs

		M_4	M_{4_cal}	M_6	M_{6_cal}
Semimajor axis length±STDs (m/s)	axis	0.15±0.05	0.15±0.07	0.11±0.04	0.07±0.02
Semiminor axis length±STDs (m/s)	axis	0.04±0.03	0.04±0.03	0.03±0.02	0.01±0.00

C. Dynamic mechanisms of residual currents

To comprehend the main dynamic processes of the residual currents in ZTYB, we decompose the depth-averaged currents ($\vec{u} = u\vec{\imath} + v\vec{\jmath}$) observed by CAT into two parts: the tidal currents ($\vec{u}' = u'\vec{\imath} + v'\vec{\jmath}$) and the residual currents ($\vec{U} = U\vec{\imath} + V\vec{\jmath}$). The momentum equation, integrated from the sea bottom to the sea surface and averaged over one tidal cycle [6], [8]-[9] can be written as

$$\nabla_h \cdot \left(\overline{\vec{u}'\vec{u}'}\right) = -g\nabla_h\bar{\eta} - \nabla_h\left(\vec{U}\vec{U}\right) + A_m\nabla_h \cdot \left(\nabla_h\vec{U}\right) + \frac{\overline{\vec{\tau}_w}}{\rho h} - \frac{\overline{\vec{\tau}_b}}{\rho h} - f\vec{k} \times \vec{U} \qquad (3)$$

here, $\vec{\imath}, \vec{\jmath}, \vec{k}$ are unit vectors in the eastward, northward, upward directions, respectively; $\nabla_h = \vec{\imath}\frac{\partial}{\partial x} + \vec{\jmath}\frac{\partial}{\partial y}$; A_m is the horizontal eddy viscosity coefficient, which is set as 90 m^2/s [10]. Overbars denote a temporal average over one tidal cycle.

The term on the left-hand side of (3) is known as the tidally averaged advection of the tidal currents [8]. It is balanced by the six terms on the right-hand side of (3). To quantify the role of each term in (3) in generating the residual current in ZTYB, the maximum and mean values of these terms are calculated during one M_2 tidal period (Table 2). The horizontal distributions of the six terms (except $-g\nabla_h\bar{\eta}$) in (3) are shown in Fig. 6a-6f.

Fig. 6a shows that the tidally averaged advection term of the tidal currents ($\left|\nabla_h \cdot \left(\overline{\vec{u}'\vec{u}'}\right)\right|$) is large where the residual current is strong, the maximum value being 3.36×10^{-4} m/s^2 near Luotou channel. The mean value in the observation region is about 1.25×10^{-4} m/s^2 (Table 2). The spatial distribution of the residual current advection term ($\nabla_h\left(\vec{U}\vec{U}\right)$) (Fig. 6b) is similar to that of $\left|\nabla_h \cdot \left(\overline{\vec{u}'\vec{u}'}\right)\right|$, with larger values near Luotou channel, and its value becomes about 2×10^{-5} m/s^2 near Fodu channel. The maximum and mean values in the observation region are 1.76×10^{-4} m/s^2 and 4.74×10^{-5} m/s^2, respectively. The mean value of $\left|\nabla_h\left(\vec{U}\vec{U}\right)\right|$ takes up 37.9% of $\left|\nabla_h \cdot \left(\overline{\vec{u}'\vec{u}'}\right)\right|$.

The spatial distribution of the time mean horizontal mixing term ($A_m\nabla_h\cdot(\nabla_h\vec{U})$) (Fig. 6c) is different from that of the first two terms, and the mean value of $|A_m\nabla_h\cdot(\nabla_h\vec{U})|$ is only about 5×10^{-7} m s^{-2}, which takes up 0.4% of $|\nabla_h\cdot(\overrightarrow{u'u'})|$. The spatial pattern of the time mean bottom friction term ($\frac{\overrightarrow{\tau_b}}{\rho h}$) (Fig. 6d) is similar to that of $|\nabla_h\cdot(\overrightarrow{u'u'})|$, with mean value about 8.1×10^{-6} m/s^2, which is about 6.5% of $|\nabla_h\cdot(\overrightarrow{u'u'})|$. The time mean wind stress term ($|\frac{\overrightarrow{\tau_w}}{\rho h}|$) (Fig. 6f) is 5.18×10^{-6} m/s^2, which is 4.2% of $|\nabla_h\cdot(\overrightarrow{u'u'})|$. The mean value of the time mean Coriolis term ($-f\vec{k}\times\vec{U}$) (Fig. 6e) is 14.6% of $|\nabla_h\cdot(\overrightarrow{u'u'})|$ (Table. 1). The CAT does not measure sea surface level in the observation region, therefore we can only estimate the time mean horizontal pressure gradient term ($-g\nabla_h\bar{\eta}$) by using (3). The results show that the mean value of $|g\nabla_h\bar{\eta}|$ in this region is about 4.55×10^{-5} m/s^2, which is about 36.4% of $|\nabla_h\cdot(\overrightarrow{u'u'})|$.

Therefore, the momentum equation (3) of the residual currents in ZTYB is mainly balanced by the tidally averaged advection of the tidal currents ($\nabla_h\cdot(\overrightarrow{u'u'})$), the averaged horizontal pressure gradient ($-g\nabla_h\bar{\eta}$) and the advection of the residual currents ($\nabla_h(\vec{U}\vec{U})$). In this region, wind stress ($\frac{\overrightarrow{\tau_w}}{\rho h}$), bottom friction ($\frac{\overrightarrow{\tau_b}}{\rho h}$) and Coriolis force ($-f\vec{k}\times\vec{U}$) play relatively less important roles, and horizontal mixing (($A_m\nabla_h\cdot(\nabla_h\vec{U})$) is negligible.

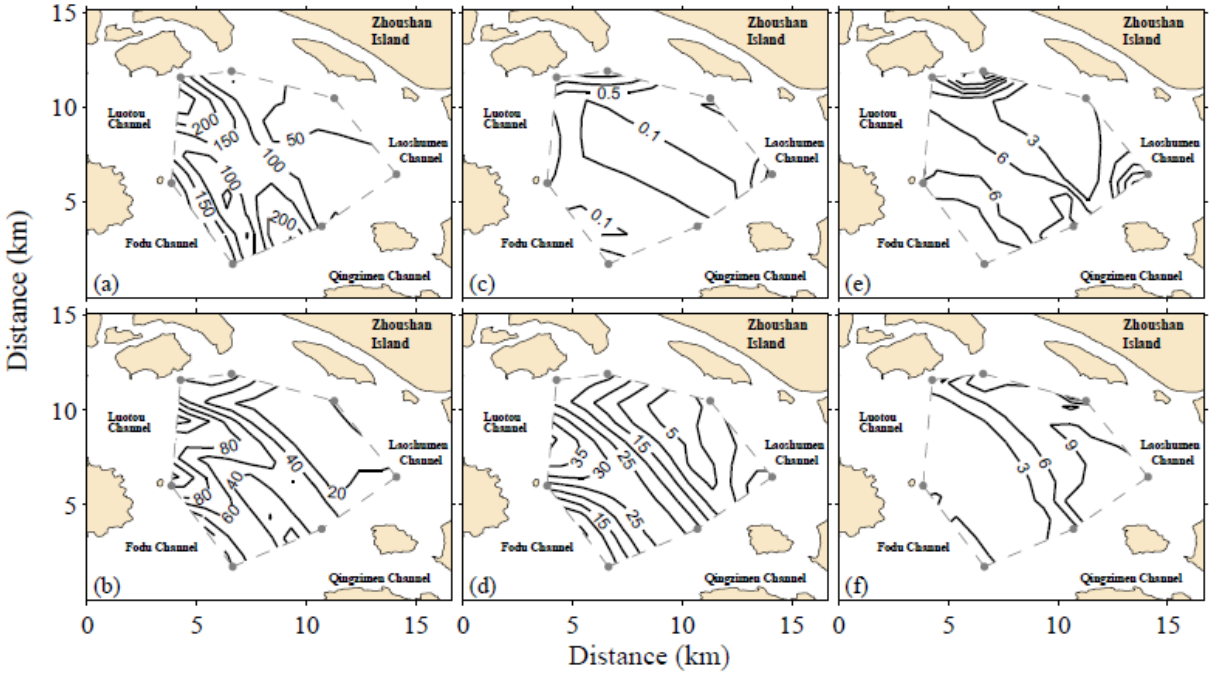

Fig. 6 Contour plot (in units of 10^{-6} m s^{-2}) for terms in (3): (a) $|\nabla_h\cdot(\overrightarrow{u'u'})|$, (b) $|\nabla_h(\vec{U}\vec{U})|$, (c) $|A_m\nabla_h\cdot(\nabla_h\vec{U})|$, (d) $|\frac{\overrightarrow{\tau_b}}{\rho h}|$, (e) $|f\vec{k}\times\vec{U}|$, (f) $|\frac{\overrightarrow{\tau_w}}{\rho h}|$.

Table 2. Maximum and average values (in units of 10^{-6} m/s^2) of dynamic terms in the tidally averaged momentum equation, and percentages of each term relative to the forcing term.

	$\lvert\nabla_h \cdot (\overline{\vec{u}'\vec{u}'})\rvert$	$\lvert\nabla_h(\vec{U}\vec{U})\rvert$	$\lvert\nabla_h \cdot (A_m \nabla_h \vec{U})\rvert$	$\left\lvert\frac{\overline{\tau_b}}{\rho h}\right\rvert$	$\lvert f\vec{k} \times \vec{U}\rvert$	$\left\lvert\frac{\overline{\tau_w}}{\rho h}\right\rvert$
Maximum value	336	176	0.08	75	48.7	11.0
Percentage,%	100	52.4	0.02	22.3	14.5	3.3
Average value	125	47.4	0.5	8.1	18.3	5.2
Percentage,%	100	37.9	0.4	6.5	14.6	4.2

IV. Summary

In this study, we use CAT data to reconstruct the horizontal distributions of tidal currents and residual currents in ZTYB. Furthermore, we also demonstrate that the overtides M_4 and M_6 are mainly generated by the nonlinear advection and quadratic bottom friction terms of M_2, respectively. All these results indicate that the M_4 and M_6 tidal currents directly measured by the CAT are credible. To the best of our knowledge, this study is the first nonlinear tidal current measurement by CAT.

We also analyze the main dynamic processes responsible for the residual currents by using the averaged horizontal momentum equation. The predominant terms in balancing the momentum equation of the residual currents are advection of the tidal currents, horizontal pressure gradient, and advection of the residual currents, while the bottom friction and Coriolis force terms contribute less.

The results show the advantages of the CAT system for accurately mapping horizontal variations of tidal currents and residual currents. Our study suggests that CAT measurements have advantages for current monitoring over a large area and understanding dynamic mechanisms in coastal regions.

V. ACKNOWLEDGEMENT

This study is supported by the National Natural Science Foundation of China (41276095, 41476020, 41576001, 41321004 and 41576031); the Scientific Research Fund of SIO under grant JT1402; the projects of the State Key Laboratory of Satellite Ocean Environment Dynamics, SIO (SOEDZZ1501); the National Programme on Global Change and Air-Sea Interaction (GASI-IPOVAI-01-02).

VI. REFERENCES

[1] H. Yamaoka, A. Kaneko, J.-H. Park, H. Zheng, N. Gohda, T. Takano, et al., “Coastal acoustic tomography system and its field application,” *IEEE Journal of Oceanic Engineering*, 27(2), pp. 283–295, 2002.

[2] X.-H. Zhu, A. Kaneko, Q. Wu, C. Zhang, N. Taniguchi, and N. Gohda,. “Mapping tidal current structures in Zhitouyang Bay, China, using coastal acoustic tomography,” *IEEE Journal of Oceanic Engineering*, 38(2), pp. 285-296, 2013.

[3] J.-H. Park, and A. Kaneko, “Computer simulation of the coastal acoustic tomography by a two-dimensional vortex model,” *Journal of Oceanography*, 57, pp. 593-602, 2001.

[4] P. C. Hansen, and D. P. O’Leary, “The use of the L-cure in the regularization of discrete ill-posed problems,” *SIAM J. Sci. Comput.*, 14(6), pp. 1487-1503, 1993.

[5] R. Pawlowicz, B. Beardsley, and S. Lentz, “Classical tidal harmonic analysis including error estimates in MATLAB using T_TIDE,” *Computers and Geosciences*, 28, pp. 929-937, 2002.

[6] X.-H. Zhu, Z.-N. Zhu, and X. Guo, “Coastal tomographic mapping of nonlinear tidal currents and residual currents,” *Continental Shelf Research*, under review.

[7] B. B. Parker, “The relative importance of the various nonlinear mechanisms in a wide range of tidal interactions (review),” In *Tidal Hydrodynamics*, Parker, B. B (Ed.), Wiley New York, USA, pp. 237-268, 1991.

[8] J. Sheng, and L.Wang, “Numerical study of tidal circulation and nonlinear dynamics in Lunenburg Bay, Nova Scotia,” *Journal of Geophysical Research*, 109, C10018, doi:10.1029/2004JC002404, 2004.

[9] X.-H. Zhu, Z.-N. Zhu, X. Guo, Y.-L. Ma, X. Fan, M. Dong, and C. Zhang, “Measurement of tidal and residual currents and volume transport through the Qiongzhou Strait using coastal acoustic tomography,” *Continental Shelf Research*, 108, 65-75, 2015.

[10] M. Cáceres, A. Valle-Levinson, and L. Atkinson, “Observations of cross-channel structure of flow in an energetic tidal channel,” *Journal of Geophysical Research*, 108 (C4), 3114, doi:10.1029/2001JC000968, 2003.